

CHAPTER III

METHODOLOGY

3.1 Material

3.1.1 NRL Foam

Natural rubber latex foam (NRLF) is a porous material exhibiting excellent mechanical properties, produced by foaming natural rubber latex followed by curing. NRLF has found widespread application in packaging materials. (Eaves. 2004). NRLF is synthesized using the Dunlop show in Figure 3.1, which involves whipping the latex into a froth, molding, and vulcanizing to achieve the desired foam structure (Blackley. 1997).

Table 3.1 Formulation of the natural rubber latex (NRL) compounds for the synthesis of reinforcing NRL foam (NRLF).

Ingredients	Content (phr ¹)	Functions
60% High ammonia natural rubber latex (HA Latex)	100.00	Matrix
10% Potassium oleate (K-oleate)	4.50	Foaming agent
50% Sulfur	2.00	Vulcanizing agent
50% Zinc diethylthiocarbonate (ZDEC)	2.00	1st accelerator
50% Zinc 2-mercaptobenzothiazone (ZDMT)	2.00	2nd accelerator
50% Wingstay L	2.00	Antioxidant
50% Zinc oxide (ZnO)	5.00	Activator
12.5% Sodium silicofluoride (SSF)	1.00	1st gelling agent
33% Diphenyl guanidine (DPG)	1.40	2nd gelling agent

¹Parts per hundred rubbers.

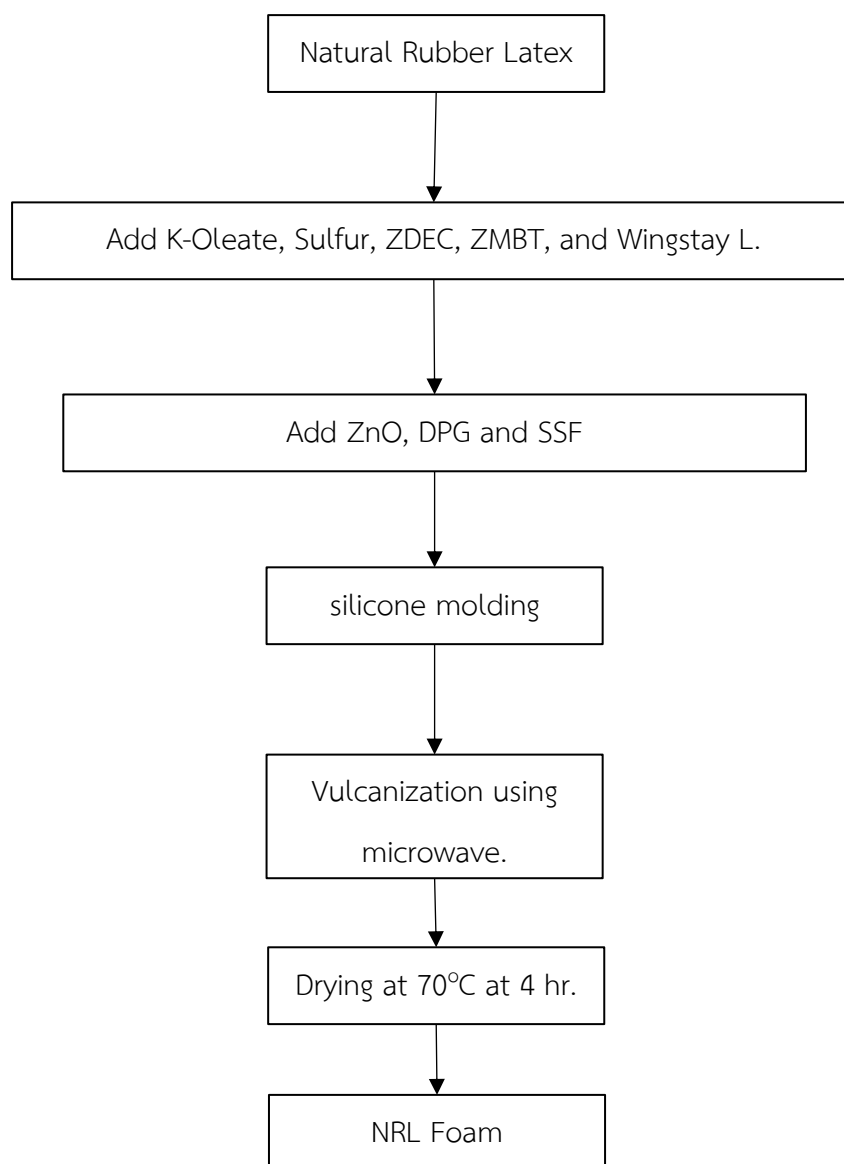


Figure 3.1 Flowchart of processing step NRL foam

3.1.2. Cushioning materials and testing

Mechanical properties were measured using a Universal Testing Machine (UTM) Instron Model 5560. A 1 kN load cell was employed, and the crosshead speed was set at 12 mm/min. Foam specimens, 3 mm thick, were cut into 100 mm × 100 mm square shapes. The compressive strength was reported at 50% strain. The cushion coefficient (C) serves as an indicator of cushioning performance, representing a material's ability to absorb energy under stress.(Xiao et al. 2022).The cushion coefficient was determined from the compressive stress-strain curve using the following equation:

Cushion coefficient. The cushion coefficient (C) is an ability of a cushion material to absorb the applied energy. The calculation was carried out using the data from the compression test mentioned earlier. The cushion coefficient equation is as follows

$$c = \frac{\sigma}{e} \times 100 \quad (23)$$

Where σ is the compressive stress (N/mm²), e is the energy absorption of the material (N·mm/mm³), which is estimated from the compressive stress–strain curve using

$$e = \int_0^e \sigma d\epsilon \quad (24)$$

Where ϵ is the compressive strain (mm/mm).

3.1.3. Testing Method

ASTM D3574 Standard Test Methods for Flexible Cellular Materials-Slab, Bonded, and Molded Urethane Foams

ASTM D3574 C is one such testing method that comprises a range of tests to specify the several properties of the foam. This consists of measurements of odor, dynamic force responses, foam density, aging, and mechanical properties.

The specified standard specimen for ASTM D3574 test C is recommended to have minimum dimensions of 50 mm in length, 50 mm in width, and 25 mm in

thickness as shown in Figure 3.2. While this represents the lower limit, it is advisable to utilize larger specimens. Ideally, the specimen's surface area should be a minimum of 2500 mm², coupled with a minimum thickness of 20 mm.



Figure 3.2 Sample cube specimen of 50 mm X 50 mm X 25 mm used in the study.

Achieving accuracy in finite element method simulations necessitates the precise definition of a material's mechanical properties

Material property using finite element methods included Modulus of elasticity, Yield stress, Poisson's ratio.

Mechanical properties were measured using a Universal Testing Machine (UTM) Instron Model 5560. The INSTRON Control module to develop systematic test methodologies for materials evaluation. The Control module enables the design of precise, multi-stage testing protocols with predefined displacement or force parameters, allowing for comprehensive material characterization under controlled conditions. The experimental apparatus utilized was the INSTRON/5565 universal testing machine, as shown in Figure 3.3, which provided the necessary mechanical precision and data acquisition capabilities required for this investigation.



Figure 3.3 Universal testing machine (INSTRON/5565, Norwood, MA, USA).

Investigation was performed on a rigid natural rubber latex foam material of density 272.06 kg/m^3 . The natural rubber latex foam specimens size used where dimension $50 \text{ mm} \times 50 \text{ mm} \times 25 \text{ mm}$ as shown in Figure 3.5

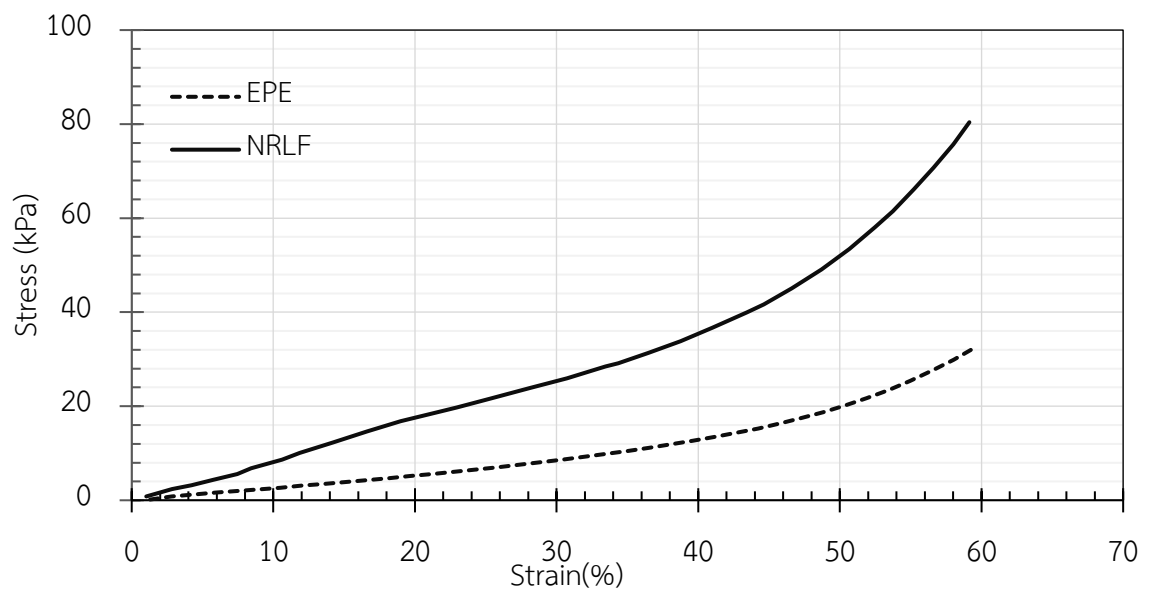


Figure 3.4 Stress-strain curve of the EPE and NRLF foam obtained using a compression test.

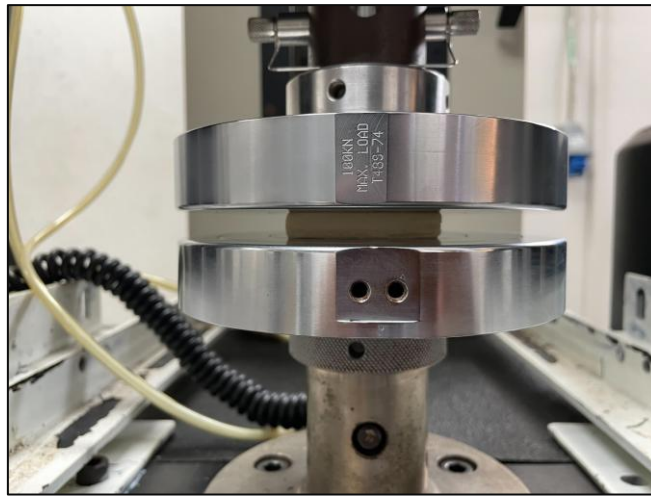


Figure 3.5 Sample cube specimen of 50 mm X 50 mm X 25 mm follower ASTM D3574 test C under compression testing.

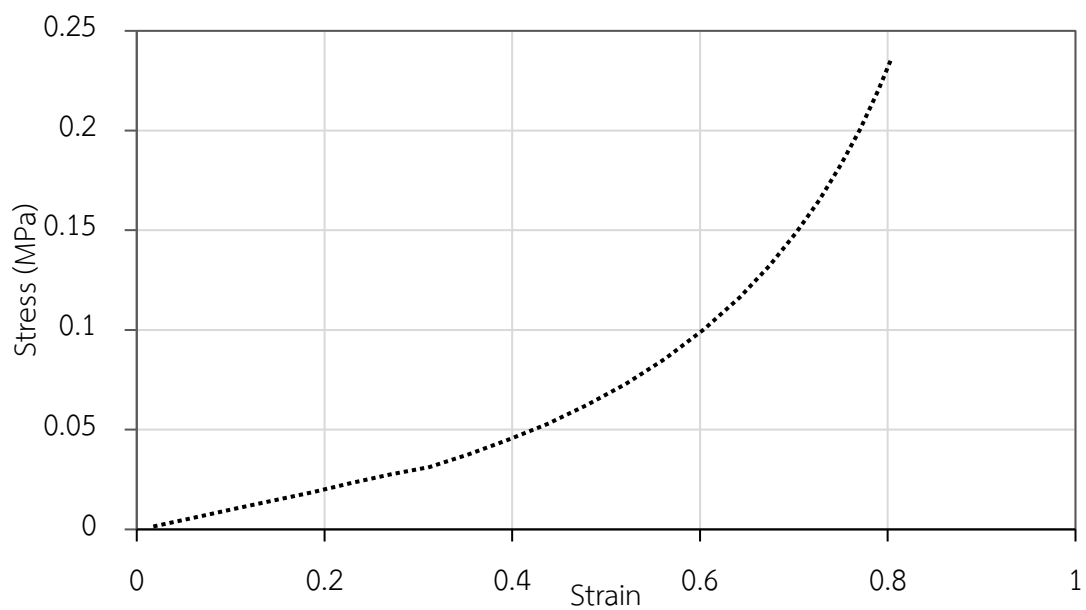


Figure 3.6 Stress-strain curve of the EPE foam obtained using a compression test.

Table 3.2 Compressive stress at 50% Strain of foam samples

Cushion foam	Compressive stress at 50% Strain (kPa)
EPE	18.75
NRLF	56.85

3.1.4. Mechanical Characterization of Guava Under Compression

Compressive testing is a fundamental mechanical characterization technique used to assess a material's ability to withstand loads that tend to reduce size. When applied to biological materials such as fruit, compressive testing provides insight into the deformation behavior, failure mechanisms, and structural integrity of the cellular matrix. In the case of guava, which has a heterogeneous internal structure comprised of soft parenchymatous tissue and denser seed cavities, the compressive response is expected to be non-linear and highly dependent on factors such as maturity, moisture content, loading rate, and orientation. The objective of this investigation is to systematically characterize the compressive behavior of guava under quasi-static loading conditions. Emphasis is placed on the influence of specimen orientation, size, and maturity on the resulting mechanical parameters.

3.1.5. Characterization of Mechanical Properties

Compressive testing represents a fundamental mechanical characterization method, widely employed to evaluate materials' resistance to externally applied loads that induce size reduction. In the context of biological materials, particularly fruits, compressive testing elucidates deformation behavior, failure mechanisms, and structural integrity of cellular matrices. Guava (*Psidium guajava* L.), known for its heterogeneous internal architecture comprising soft parenchymatous tissue surrounding comparatively denser seed cavities exhibit complex, non-linear compressive responses. This behavior is strongly influenced by factors such as fruit maturity, moisture content, loading orientation, and strain rate.

In this investigation, the compressive behavior of the 'Glom Sali' guava cultivar was systematically characterized under quasi-static loading conditions. Particular emphasis was placed on the influence of sample orientation, maturity level, and geometric parameters on the resulting mechanical responses. To support finite element modeling of guava deformation, both physical and mechanical properties were experimentally determined.

A total of ten mature guava fruits, each weighing between 250 and 300 grams, were randomly selected for preliminary characterization. The average density and volume were determined to be 1.24 ± 0.07 g/mL and 194.6 ± 17.73 mL, respectively. The measured average horizontal width and vertical length were 7.5 cm and 8.0 cm, respectively, with a mean fruit weight of 239.1 g. Additional mechanical parameters, such as firmness (4.68 N), were recorded to facilitate the estimation of material stiffness. Key physical attributes—including diameter, uniformity, and maturity were also documented, as these parameters directly influence mechanical response under compressive loading.

For compression testing, cubic specimens with dimensions of 20 mm x 20 mm were extracted from the equatorial region of the fruit (Figure 3.7).

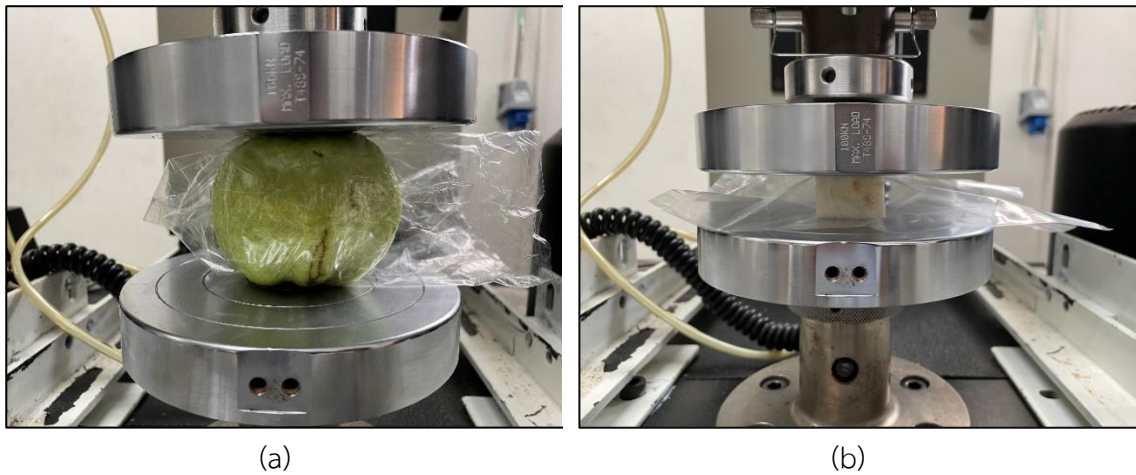


Figure 3.7 (a) Guava fruit (*Psidium guajava* L.) cv. Glom Sali (b) Sample cube specimen of guava (*Psidium guajava* L.) using in the present study sample size 20 mm x 20 mm.

Young's modulus (Y) was determined by measuring the equatorial diameter of the fruit (d) and subsequently substituting this value into the following equation.

$$Y = \frac{\sigma}{\epsilon} \quad (25)$$

Where: $\sigma = \frac{4F}{\pi d^2}$, $\epsilon = \frac{d_i - d_f}{d_i}$ the strain of the guava,

σ is a measure of the force acting on a unit area of a material

ϵ is the deformation of a material from stress

d_i is equatorial diameter of the deformed fruit

d_f is equatorial diameter of the intact fruit

Alternatively, the acoustic impact test can be utilized to determine Young's modulus by incorporating the values of fruit firmness (Sc) and density (ρ) into the following equation.

$$Y = Sc \rho^{1/3} \quad (26)$$

Where: Sc is the stiffness coefficient ($\text{Kg}^{2/3}/\text{s}^2$), f the dominant resonant frequency where the response magnitude is greatest (Hz) and m the fruit mass (g).

The Sc is significantly correlated with fruit firmness and sensory measurements (Galili and De Baerdemaeker 1996).

$$Sc = f^2 m^{2/3} \quad (27)$$

The stress-strain profile obtained from quasi-static compression tests (Figure 3.8) demonstrates the inherently non-linear response of guava tissue under load. The initial elastic regime is followed by a yielding region and subsequent densification, typical of porous, viscoelastic biological materials. These experimentally derived parameters are intended to inform and calibrate the finite element model simulating internal stress distribution and failure propagation within the guava matrix.

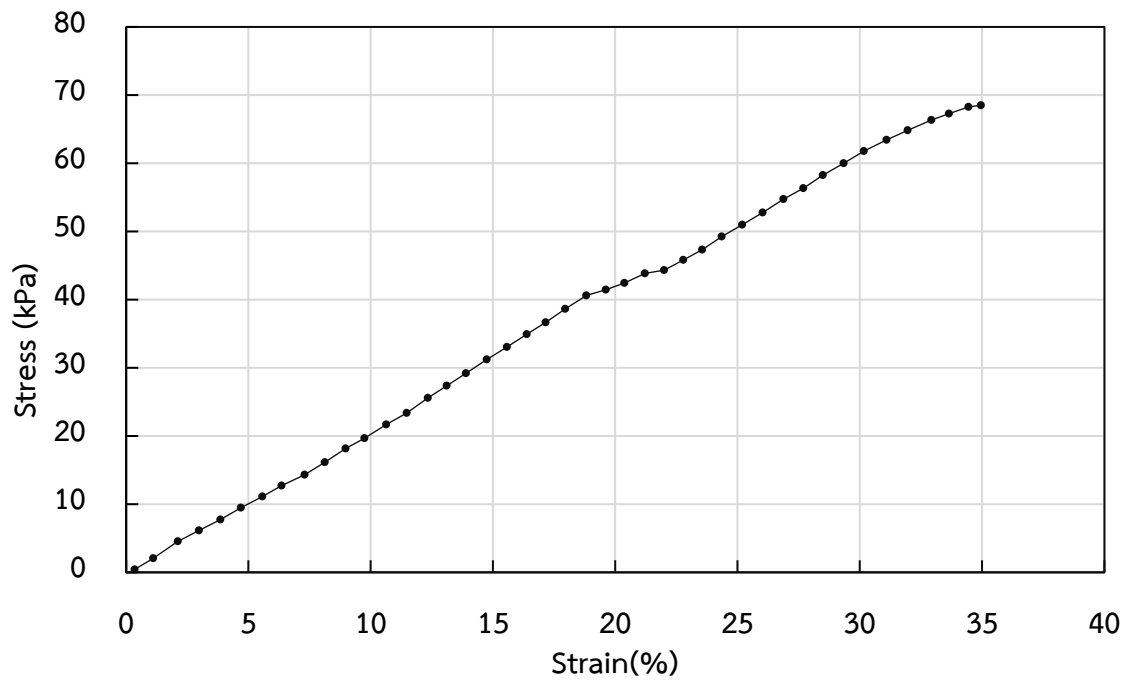


Figure 3.8 Stress-strain curve of the Guava (*Psidium guajava* L.) obtained using a compression test.

3.1.6. Poisson's ratio

Negative Poisson's ratio

The Poisson's ratio of a material describes the relationship between the transverse strain (expansion or contraction in the horizontal direction) and the axial strain (extension or compression in the vertical direction as shown in Figure 3.9).

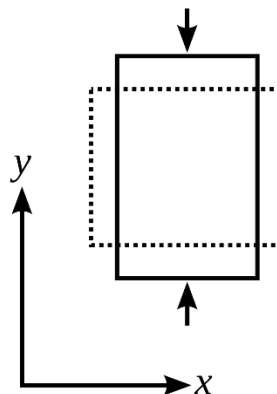


Figure 3.9 The Poisson's ratio of a material

The x-axis, with a Poisson's ratio of 0.5. The original green cube experiences no strain, while the red cube undergoes an expansion of ΔL in the x direction due to tension. Simultaneously, it contracts in the y and z directions by $\Delta L'$ as shown in Figure 3.10

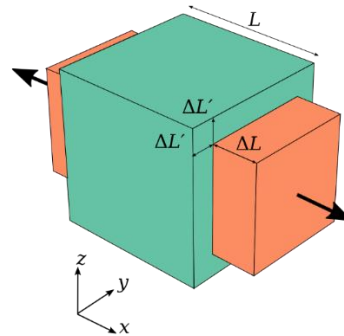


Figure 3.10 A cube made of an isotropic linearly elastic material is stretched along

Schematic explanation of the two-dimensional Poisson effect. **(A)** A two-dimensional depiction of an elastic material. **(B–D)** Schematic depictions about how the material **(A)** deforms under **(B)** horizontal stretching, **(C)** vertical squashing, and **(D)** vertical stretching from the top. Each depiction is accompanied by related horizontal and vertical deformation vectors shown in Figure 3.11 (Vijayakumar et al. 2021).

	A No applied force	B Horizontal stretching	C Vertical squashing	D Vertical stretching from top
Material deformation				
Horizontal deformation vectors				
Vertical deformation vectors				

Figure 3.11 Schematic explanation of the two-dimensional poisson effect

Poisson's ratio of material

Samples used for Tests Guava consisted of dimensions of 15 mm x 15 mm with a thickness of 20 mm as shown in Figure 3.12. The compression speed 5 mm/min stop at 50% strain the as shown in Table 3.3.

$$\nu = \frac{-\varepsilon_x (\text{Lateral strain})}{\varepsilon_z (\text{Longitudinal strain})} \quad (28)$$

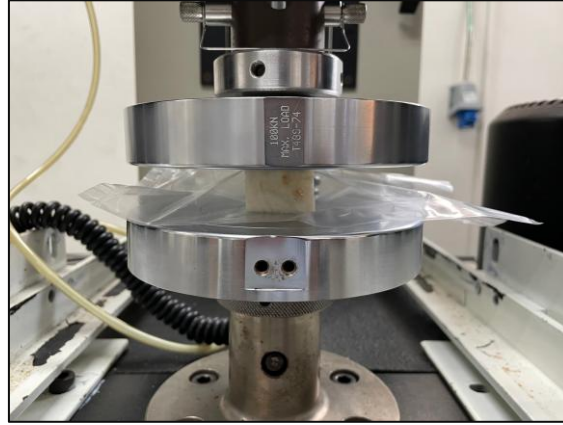


Figure 3.12 Sample cube specimen of guava (*Psidium guajava* L.) using in the present study sample size 20 mm x 20 mm.

Samples used for Tests NRLF consisted of dimensions of 20 mm x 20 mm with a thickness of 25 mm. Compression speed 50 mm/min stop at 50% strain the force displacement curve show in Figure 3.13.

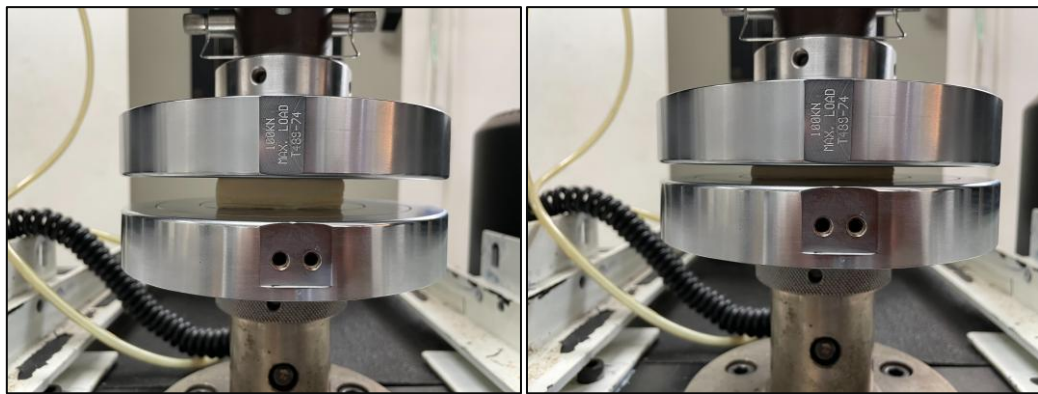


Figure 3.13 Determine of NRLF negative Poisson's ratio using UTM.

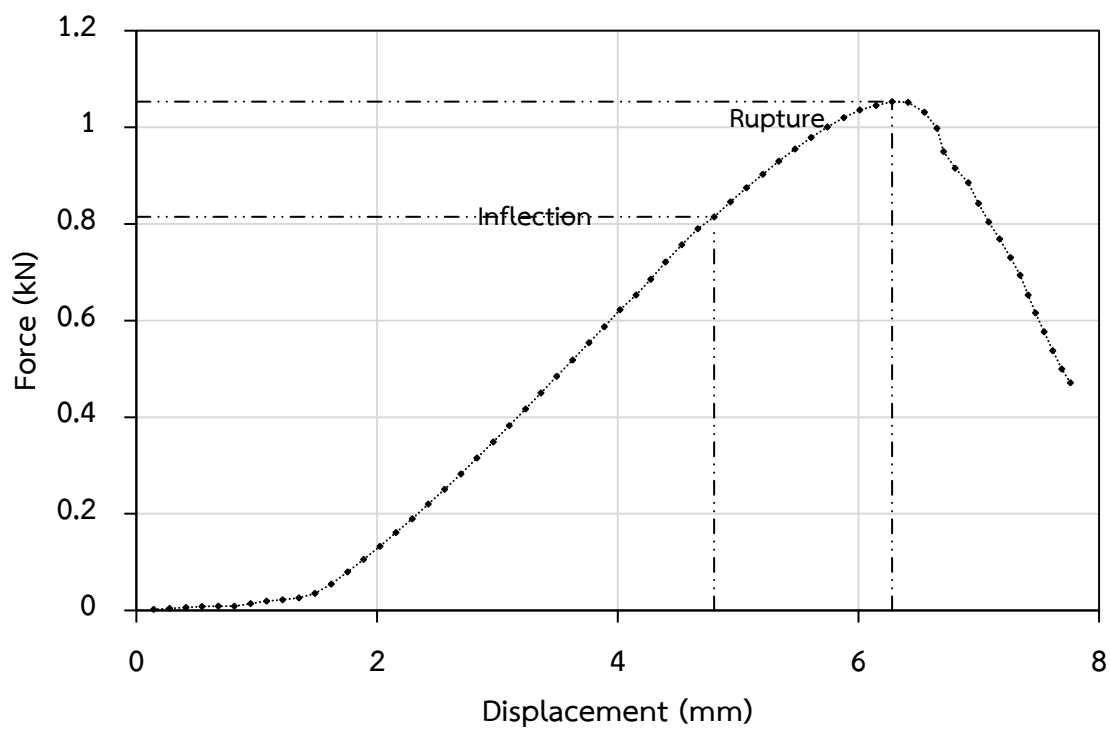


Figure 3.14 Force displacement curve of Guava fruit (*Psidium guajava* L.) Glom Sali

Table 3.3 Mechanical properties of foam samples and guava

Sample	Density ρ (Kg/m ³)	Compress stress at $\epsilon_{50\%}$ (kPa)	Young's modulus Y , (KPa)	Poisson's ratio ν
EPE	118±1.810	20.13±2.130	39.977	0.330±0.105
NRLF	272.06±3.450	56.85±3.560	105.482	0.337 ± 0.153
Guava	1240±0.070	53.53±28.320	20.739±10.242	0.490 ± 0.023

3.2 Computer-aided design

This section presents the problem simulation of drop test of guava with cushion net foam using ANSYS simulation and modeling 3D-model using Solid Work software.

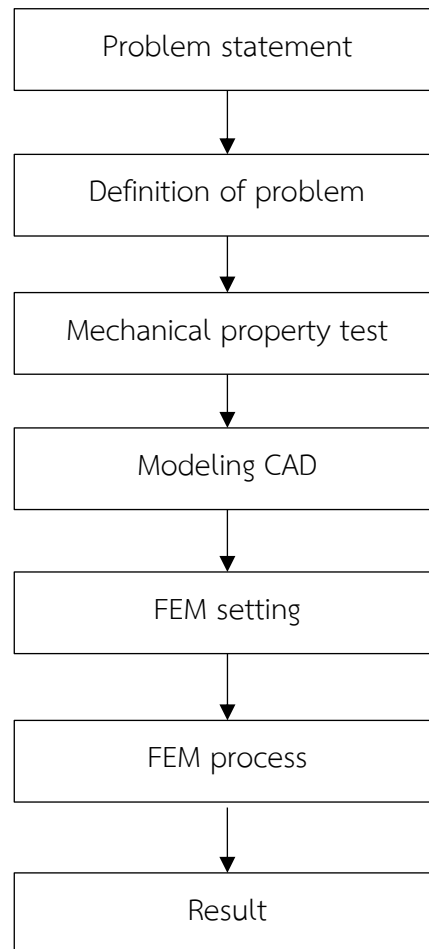


Figure 3.15 Flow chart of CAD/CAE design analysis (Chang. 2013).

3.3 Finite element analysis

3.3.1. Model Analysis

In the development of a reliable finite element model for evaluating fruit cushioning systems, the accuracy of the geometric representation is of paramount importance. This chapter presents the CAD modeling procedure for the guava fruit covered with a commercial expanded polyethylene (EPE) Figure 3.16 foam net, alongside

the design of an alternative natural rubber latex foam (NRLF) net structure. Given the complex nature of foam materials, appropriate simplifications were introduced to balance model fidelity with computational efficiency. Key geometric parameters were obtained from direct measurements and product specifications to ensure that the models accurately reflect the physical configurations used in real-world applications. The resulting CAD models serve as the foundational inputs for subsequent finite element analyses focused on impact performance



Figure 3.16 Guava with commercial expanded polyethylene foam net CAD Modeling
NRLF net foam cushion

3.3.2. Preprocess

The CAD modeling process began with the digital reconstruction of the guava's external geometry. A simplified spherical approximation was adopted to represent the guava, based on an average diameter measured from sampled fruits. The foam net was subsequently modeled by wrapping the guava with a network of interconnected struts, forming a lattice-like protective layer. For the commercial EPE foam net, standard cell shapes and connection patterns were replicated using a periodic unit cell approach. The alternative NRLF net was similarly designed but with adjusted cell dimensions and strut thicknesses to reflect the mechanical properties of the proposed material. The entire modeling process was conducted using SolidWorks® 2024, with attention to ensuring compatibility with finite element preprocessing software.

3.3.2.1 Geometry

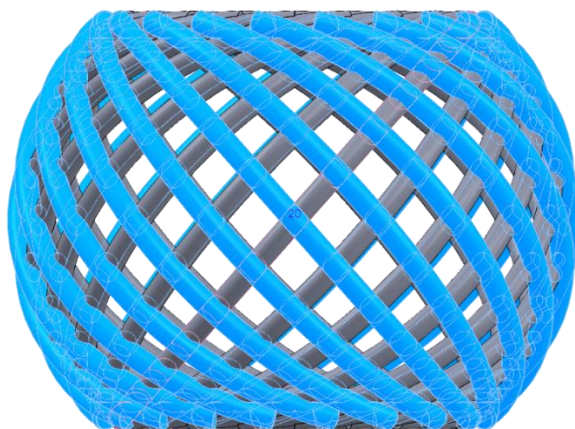


Figure 3.17 CAD cushion foam net 20 mesh filament number on NRLF 3.5 mm

3.3.2.2 CAD modeling

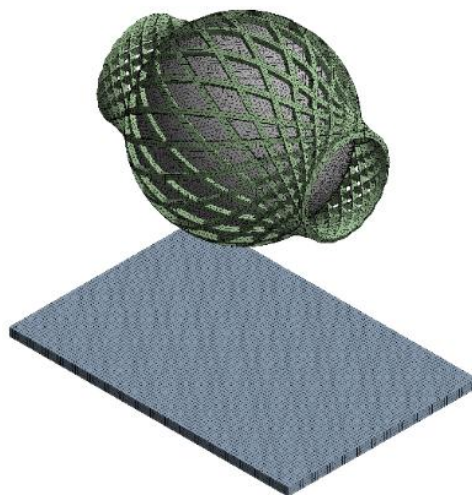


Figure 3.18 CAD model guava with expanded polyethylene cushion foam net

Simplifications and Assumptions

Several simplifications and assumptions were employed to facilitate the modeling process without compromising the essential mechanical behavior as shown in Figure 3.19

Guava Geometry: The natural irregularities of guava surfaces were neglected, and the fruit was modeled as a perfect sphere.

Foam Net Structure: The foam net was represented as a regular lattice of uniform cells, ignoring minor manufacturing imperfections.

Material Homogeneity: Both the EPE (Figure 3.20) and NRLF nets were assumed to be homogeneous and isotropic in their respective material properties.

Boundary Contact: The net was modeled to conform tightly to the guava surface, assuming perfect contact without significant gaps or slack.

Symmetry: Symmetry considerations were used wherever possible to reduce the computational domain and simulation complexity.

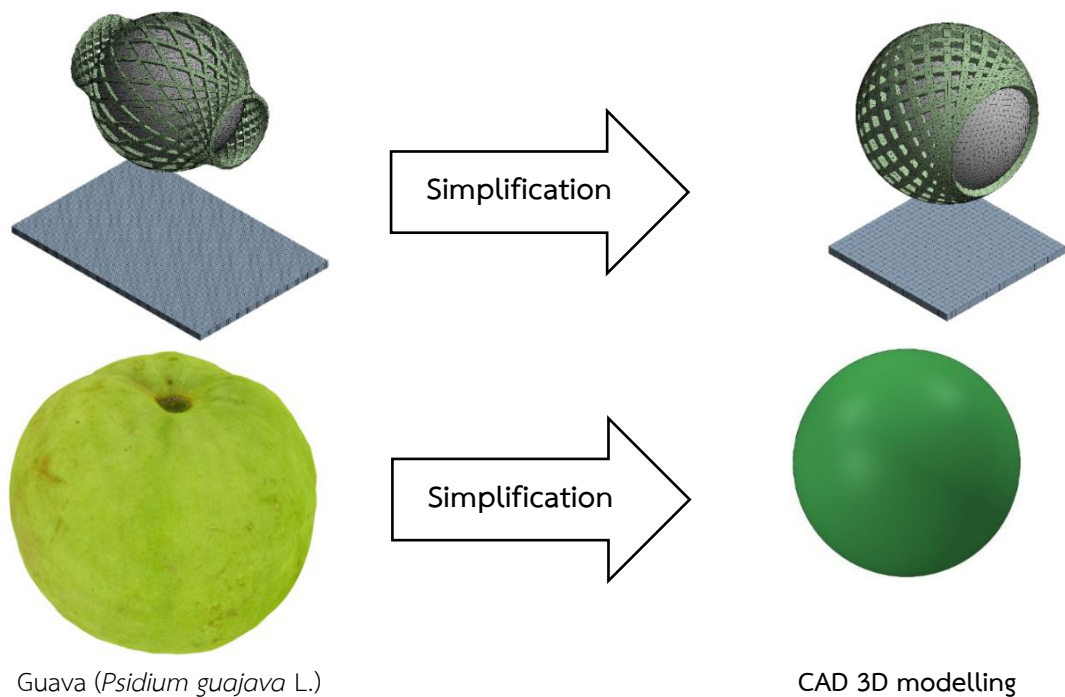


Figure 3.19 Simplifications of simulation model

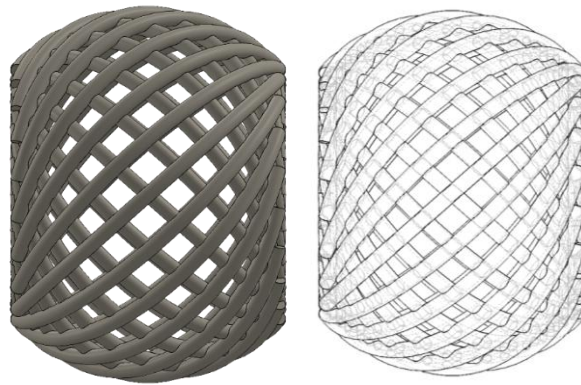


Figure 3.20 3D model of commercial cushion foam net

Parameter design of cushion net foam

Accurate parameter design is essential for optimizing the protective performance of cushioning systems. This chapter presents a comprehensive study on the parameterization and finite element method (FEM) simulation of Natural Rubber Latex Foam (NRLF) net structures intended for guava impact protection. The analysis investigates the effects of three principal parameters on the cushioning efficiency: filament diameter, filament number, and foam density. Three levels of filament diameter 2.5 mm, 3.5 mm, and 4.5 mm were considered, along with filament numbers of 15, 20, and 25 arranged across the net structure. Foam densities of 345 kg/m³, 397 kg/m³, and 420 kg/m³ were also examined to assess their influence on mechanical behavior.

CAD models corresponding to different filament numbers (15, 20, and 25) with a constant filament diameter of 3.5 mm were developed, as illustrated in Figure 3.21.




CAD Model			
Filaments number	15	20	25

Figure 3.21 CAD 3D model filament dimension 3.5 mm (number a:25, b: 20, and c: 15 filament)

3.3.2.3 Boundary Conditions (BCs)

Establishing appropriate boundary conditions (BCs) is crucial for accurately simulating the mechanical response of a guava fruit enclosed within cushioning packaging during impact scenarios. In this study, the guava, encased within either a commercial expanded polyethylene (EPE) net (Figure 3.22) or a Natural Rubber Latex Foam (NRLF) net, was modeled as undergoing free fall under the influence of gravitational acceleration. The simulation setup reflects a drop impact where the fruit-packaging assembly falls freely and strikes a rigid surface. To represent the ground contact, a planar fixed support was defined, constraining all translational and rotational degrees of freedom. Gravitational force was applied uniformly to the entire assembly to replicate natural free-fall conditions Table 3.4. These Material Definitions setting show in Table 3.5 and boundary conditions were carefully designed to mirror experimental setups commonly used in drop impact testing and to ensure realistic energy transfer and stress development upon collision.

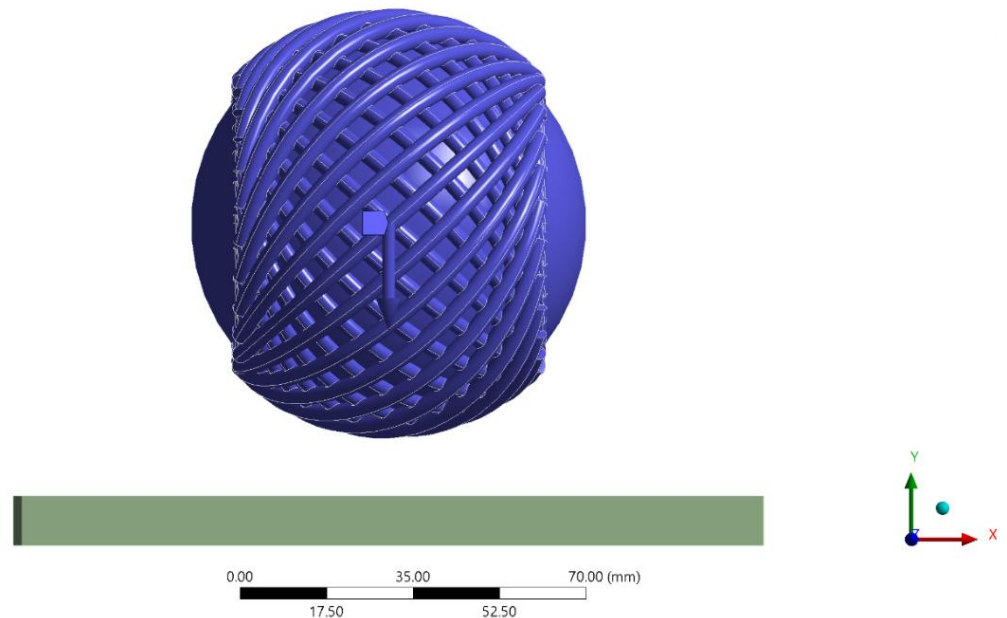


Figure 3.22 FEM model for simulating with the impact plane drop test.

Standard earth gravity direction at Drop height

$$mgh_1 = \frac{mv_1^2}{2} = mgh_2 = \frac{mv_2^2}{2} \quad (29)$$

The velocity calculated with $v_2 = \sqrt{2g(h_1 - h_2)}$

Table 3.4 Direction of setting standard earth gravity

Direction	Gravity
X component	0.00 mm/s ²
Y component	-9806.60 mm/s ²
Z component	0.00 mm/s ²

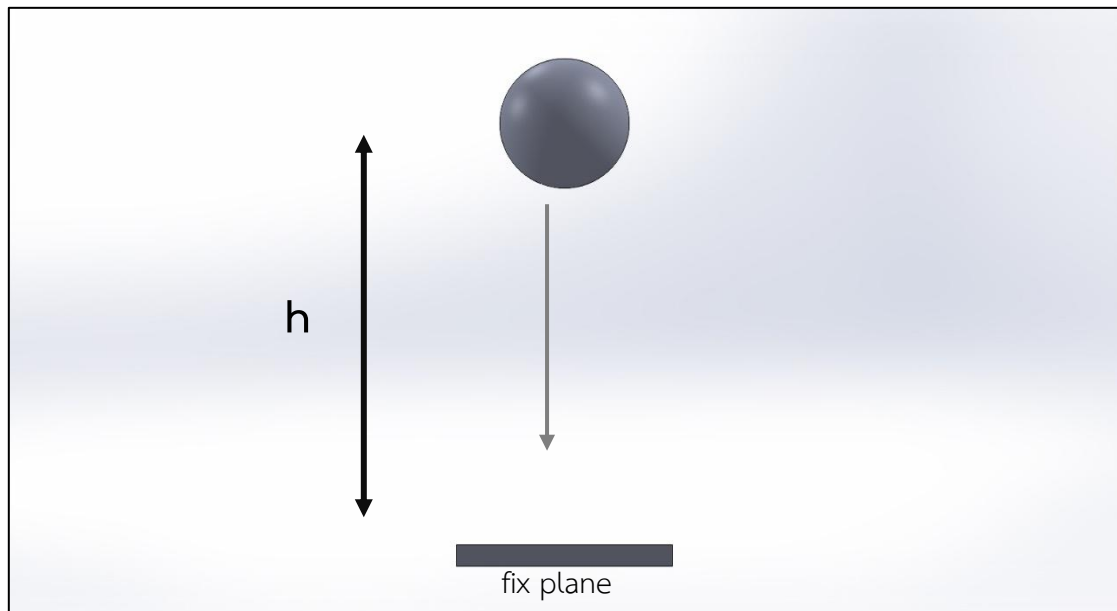


Figure 3.23 FEM model boundary conditions drop high setting

3.3.2.4 Material Definition

Table 3.5 Material parameters

Sample	Density ρ (Kg/m ³)	Compressive stress (kPa)	Young's modulus Y , (KPa)	Poisson's ratio ν
EPE	118.000	20.130	39.977	0.330
NRLF	272.060	56.850	105.482	0.330
Guava	1240.000	53.530	29.739	0.490

3.3.2.5 Mesh

Mesh generation represents a fundamental step in finite element analysis (FEA), directly influencing the accuracy, stability, and computational efficiency of the simulation. In this study, a high-quality mesh was developed for the guava and cushioning net assemblies to ensure reliable prediction of mechanical responses during drop impact events. The meshing strategy involved the use of tetrahedral elements for complex geometries, with refinement applied to critical regions such as the contact interfaces between the guava and the foam net, and the areas anticipated to experience high stress concentrations. Mesh sensitivity analyses were performed to determine an optimal balance between solution accuracy and computational cost. Appropriate element sizing, and convergence criteria were established to guarantee the numerical stability of the simulation results. This meshing approach aimed to faithfully capture deformation, stress distribution, and contact behavior under dynamic loading conditions. **Error! Reference source not found.** shown the finite element model d eveloped for the simulations. the meshing methods and assigned element sizes for each component, are summarized in Table 3.6.

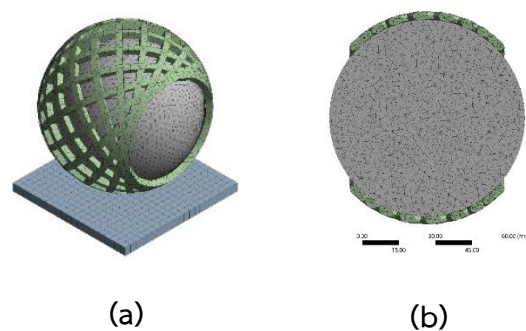


Figure 3.24 Finite element model (a) reverse-engineered guava cushion foam net model, outer mesh structure, (b) inner mesh structure)

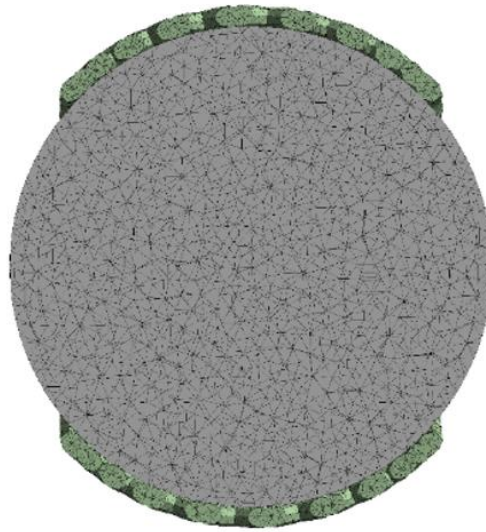


Figure 3.25 Show cross section in meshing setup of EPE cushion net foam 3.5X25 mm and guava mesh size 3.00mm

Table 3.6 Mesh method and element size

Body	Method	Element size(mm.)
Net foam	Tetrahedrons	3.00
Guava	Tetrahedrons	3.00
Impact plane	Hex Dominant	5.00

3.3.2.6 Mesh Convergence

In finite element analysis (FEA), *convergence* refers to the process of achieving a numerical solution that approximates the exact solution of the governing partial differential equations (PDEs) as the discretization of the spatial domain becomes increasingly refined (Zienkiewicz and Taylor, 2005). Mesh convergence is typically carried out by decreasing the element size and observing the effects on the solution's accuracy.

Finer mesh resolutions allow for a more accurate representation of the physical behavior across the domain, as they sample the geometry more thoroughly. However, increased accuracy often results in significantly higher computational costs, including greater memory usage and longer simulation runtimes (Cook et al., 2002). As

such, mesh convergence studies are essential for determining an appropriate balance between computational efficiency and solution accuracy (Bathe, 1996).

This FEM simulation investigates the effect of element size on the accuracy of stress predictions. The goal is to determine an optimal element size that minimizes the difference between the solution stress and the stress obtained from a finer mesh. The target is to achieve a stress difference of less than 5% shown in Figure 3.27 compared to the finer mesh solution. However, the global edge length in the current mesh is already smaller than 4.00 mm. This model uses NRLF foam net study 3.5mm 25x25, the statistics shown in

Figure 3.26 . sensitivity analysis test statistics shown in Figure 3.27.

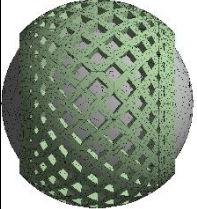
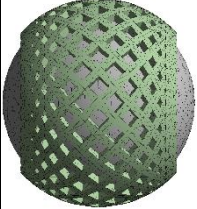
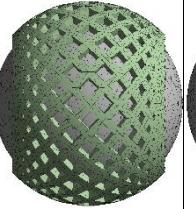
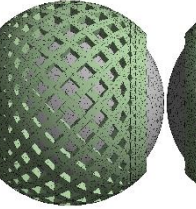
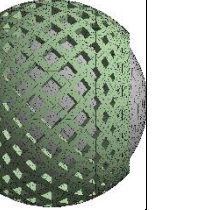
Model					
Mesh size	7.0mm.	6.0 mm.	5.0 mm.	4.0 mm.	3.0 mm.
Nodes	11287	10798	16449	20896	35584
Elements	20908	25278	28382	33061	51891

Figure 3.26 Effect of mesh size, Nodes, and elements on CAD model of NRLF cushion net foam 3.5 mm 25x25

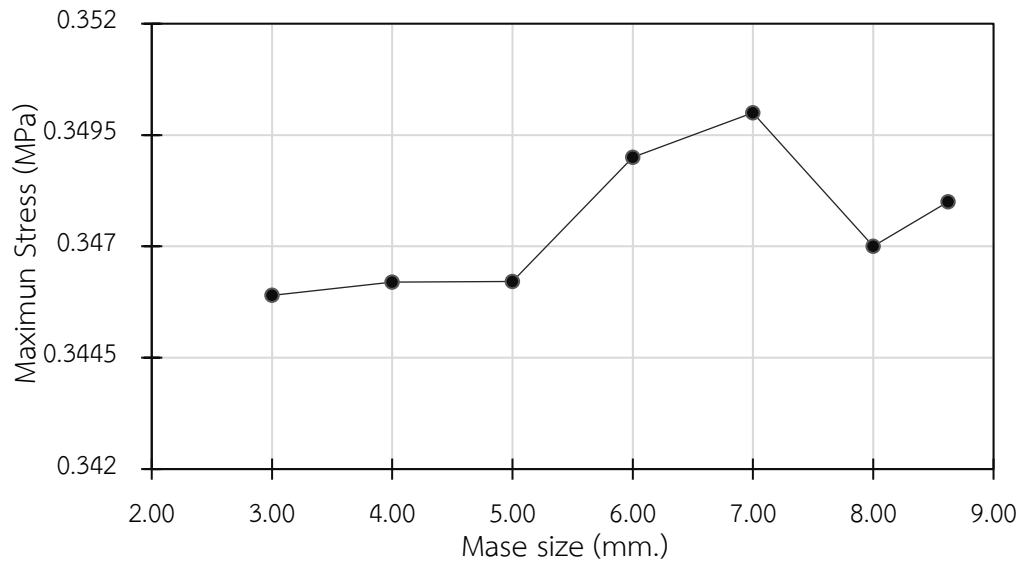


Figure 3.27 Mesh sensitivity analysis

3.3.2.7 Convergence rate

To investigate the effect of mesh refinement on the model's accuracy and computational efficiency, presents a summary of element sizes used in the NRLF net foam model with a 3.5 mm filament diameter and a 25 × 25 arrangement. As the element size is gradually reduced, the number of elements and nodes increases, leading to finer mesh resolution and a better approximation of the geometry and stress distribution. However, this increase in resolution also results in higher computational demands. The selected element size of 3.0- 4.0 mm represented an optimal balance between accuracy and computational feasibility for the simulation.

3.3.2.8 Controlling discretization error

Convergence error

$$\text{Convergence error} = \left| \frac{\text{result}(n) - \text{result}(n-1)}{\text{result}(n)} \right| \quad (30)$$

Solution error

$$\text{Solution error} = \left| \frac{\text{FE result} - \text{asymptotic result}}{\text{FE result}} \right| \quad (31)$$

Tabel 3.7 Mesh convergence

Mesh size	Elements	Nodes	Convergence error
7.0	20908	11287	-
6.0	25278	10798	33%
5.0	28382	16449	25%
4.0	33061	20896	13%
3.0	51891	35584	4%

3.4 Validation

To validate the predictive accuracy of the developed finite element model (FEM) shown in Figure 3.29, the simulated bruise areas were compared against experimental results obtained from drop tests of guava fruits without any cushioning material. The experimental data were adapted from the study by (Saengwong-Ngam et al. 2024)., which evaluated the impact protection performance of natural rubber latex foam composites reinforced with bamboo leaf fiber. The experimental procedure involved dropping the fruits from heights of 200 mm, 300 mm, and 400 mm shown in

Figure 3.28 after four days of storage, with the resulting bruise areas measured as 111.7 mm², 150.1 mm², and 216.4 mm², respectively. The FEM was constructed to replicate the experimental conditions precisely, simulating the free-fall impact of the guava fruits onto a rigid surface without protective cushioning. The comparison of the experimental and simulated bruise areas is presented in drop test simulation. Drop test simulation setup

Table 3.8 Material properties for the drop test simulation analysis

Component	Modulus of Elasticity, E (MPa)	Poisson's ratio	Mass (g)
Stainless -steel ball	200000	0.31	250
Guava	0.105	0.33	250
Plane	200000	0.30	2077.2

The entire computational domain consisted of 4,565 nodes and 22,154 elements. A Tetrahedron mesh was employed for all components to ensure accurate capture of contact interactions and deformation behavior. The mesh sizing was assigned as follows: 6 mm for the stainless-steel ball, 8 mm for the plane beneath the guava, and 10 mm

The stainless-steel ball and the guava were initially positioned above the plane at a specified drop height. Both components were assigned an initial velocity of zero prior to release, with gravitational acceleration applied uniformly in the negative y-axis direction to simulate free-fall motion.

The bottom surface of the supporting plane was fully constrained in all translational degrees of freedom (fixed support) to prevent any movement during the impact event.

No constraints were imposed on the stainless-steel ball or the guava in order to allow free motion until contact initiation occurred.

An explicit dynamic analysis was employed due to the highly nonlinear behavior associated with impact events and large deformation responses, particularly in the guava specimen, which exhibited low stiffness and viscoelastic-like characteristics.

This boundary condition setup ensured that the simulation closely represented the experimental setup used for validation, thereby enabling a direct comparison between simulated and observed deformation behaviors under drop test conditions.

Table 3.9 The entire computational domain consisted of 4,565 nodes and 22,154 elements. A Tetrahedron mesh was employed for all components to ensure accurate capture of contact interactions and deformation behavior. The mesh sizing was assigned as follows: 6 mm for the stainless-steel ball, 8 mm for the plane beneath the guava, and 10 mm

The stainless-steel ball and the guava were initially positioned above the plane at a specified drop height. Both components were assigned an initial velocity of zero prior to release, with gravitational acceleration applied uniformly in the negative y-axis direction to simulate free-fall motion. The bottom surface of the supporting plane was fully constrained in all translational degrees of freedom (fixed support) to prevent any movement during the impact event. No constraints were imposed on the stainless-steel ball or the guava in order to allow free motion until contact initiation occurred.

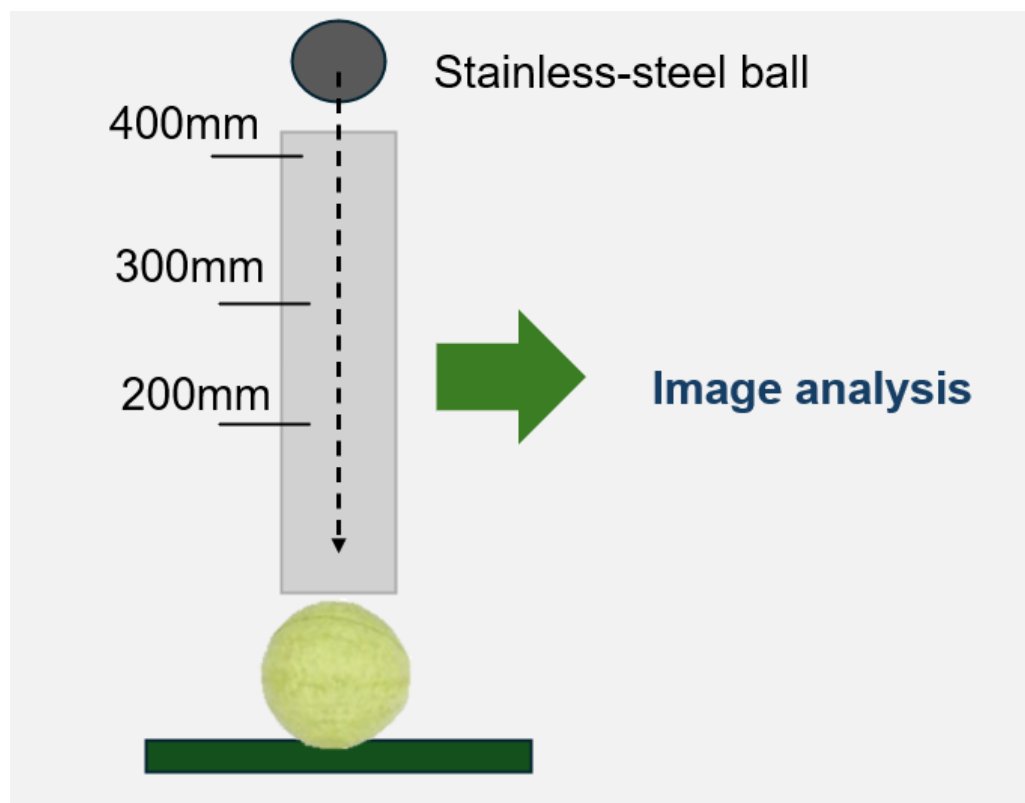


Figure 3.28 The experimental fruit bruise damage

3.4.1. Boundary Conditions Setting for Validation of Drop Test Model

In the finite element simulation of the drop test validation, appropriate boundary conditions were defined to accurately replicate the physical behavior of the system during impact. The model comprised three primary components: a stainless-steel ball, a guava specimen, and a supporting plane, each characterized by specific material properties as summarized in Table 3.8

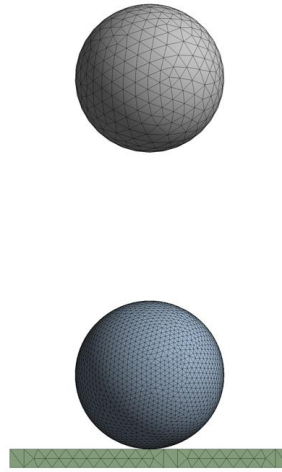


Figure 3.29 Validation model using FEM Drop test simulation setup

Table 3.8 Material properties for the drop test simulation analysis

Component	Modulus of Elasticity, E (MPa)	Poisson's ratio	Mass (g)
Stainless -steel ball	200000	0.31	250
Guava	0.105	0.33	250
Plane	200000	0.30	2077.2

The entire computational domain consisted of 4,565 nodes and 22,154 elements. A Tetrahedron mesh was employed for all components to ensure accurate capture of contact interactions and deformation behavior. The mesh sizing was assigned as follows: 6 mm for the stainless-steel ball, 8 mm for the plane beneath the guava, and 10 mm

The stainless-steel ball and the guava were initially positioned above the plane at a specified drop height. Both components were assigned an initial velocity of zero prior to release, with gravitational acceleration applied uniformly in the negative y-axis direction to simulate free-fall motion.

The bottom surface of the supporting plane was fully constrained in all translational degrees of freedom (fixed support) to prevent any movement during the impact event.

No constraints were imposed on the stainless-steel ball or the guava in order to allow free motion until contact initiation occurred.

An explicit dynamic analysis was employed due to the highly nonlinear behavior associated with impact events and large deformation responses, particularly in the guava specimen, which exhibited low stiffness and viscoelastic-like characteristics.

This boundary condition setup ensured that the simulation closely represented the experimental setup used for validation, thereby enabling a direct comparison between simulated and observed deformation behaviors under drop test conditions.

Table 3.9 Comparison of experimental and simulated bruise areas

Drop Height (mm)	Experimental Bruise Area (mm ²)	Simulated	
		Surface displacement (mm ²)	Different (%)
200	111.7	107.9	3.5
300	150.1	146.8	2.4
400	216.4	209.7	3.2

Despite these errors, the study concludes that the FEM model successfully captured the general trend of increasing bruise area with greater drop heights. This means that while the exact numerical values might have discrepancies, the model correctly predicted that higher drops would lead to larger bruise areas, which is a crucial aspect of its predictive capability.

The results confirm that the finite element model is capable of reasonably predicting the impact-induced damage behavior of guava fruits under free-fall conditions without cushioning. This validation is significant because it establishes the model as a reliable tool for further research. Consequently, the validated model can now be utilized

for further simulations involving the application of protective cushioning materials. This implies that researchers can use this model to virtually test different cushioning designs and materials to reduce impact damage, saving time and resources that would otherwise be spent on physical experiments.